MEG Source Localization using the Source Affine Image Reconstruction (SAFFIRE) Algorithm

Mihai Popescu, *Member, IEEE,* Shannon D. Blunt, *Senior Member, IEEE,*
Tszping Chan, *Student Member, IEEE*

Abstract— **Non-parametric iterative algorithms have been previously proposed to achieve high-resolution, sparse solutions to the bioelectromagnetic inverse problem applicable to multi-channel MEG and EEG recordings. Using a minimum mean-square error (MMSE) estimation framework we propose a new algorithm of this type denoted as Source Affine Image Reconstruction (SAFFIRE) aiming to reduce the vulnerability to initialization bias, augment robustness to noise, and decrease sensitivity to the choice of regularization. The proposed approach operates in a normalized leadfield space and employs an initial estimate based on matched filtering to combat the potential biasing effect of previously proposed initialization methods. SAFFIRE minimizes difficulties associated with the selection of the most appropriate regularization parameter by using two separate loading terms: a fixed noise-dependent term that can be directly estimated from the data and arises naturally from the MMSE formulation, and an adaptive term (adjusted according to the update of the source estimate) that accounts for uncertainties of the forward model in real experimental applications. We also show that a non-coherent integration scheme can be used within the SAFFIRE algorithm structure to further enhance the reconstruction accuracy and improve robustness to noise.**

***Index Terms*— MEG, inverse problem, MMSE**

I. Introduction

The non-invasive MEG recordings of extra-cranial magnetic fields provide the opportunity to study electrical neuronal activity with high temporal resolution. However, the estimation of neuronal sources from multi-channel data is complicated by the non-uniqueness of the electromagnetic inverse problem [1], the limited number of sensors, and the presence of noise in the measurements. Different approaches, which can be categorized by the specific constraints enforced on the sources, have been adopted to unambiguously select a solution. Among these, distributed source models assume the locations of a large number of dipoles to be fixed, while their amplitudes and orientations are estimated from the measured data. The large number of potential source locations yields a highly underdetermined inverse problem and requires additional (explicit or implicit) constraints to select a unique solution. The most popular approach is the minimum-norm estimate (MNE), which seeks a minimum ℓ_2 norm current distribution that explains the measured data [2,3]. A drawback of MNE is a localization bias towards the outer brain surface [4,5]. To alleviate this effect, leadfield normalization strategies denoted as normalized-MNE (nMNE) [6,7] have been employed, though this approach was found to likewise elicit a localization bias throughout the source space [5,7,8]. Other methods rely on weighted-MNE strategies [9,10]. In particular, the standardized low-resolution electromagnetic tomography (sLORETA, [10]) has been shown to provide unbiased localization of single sources [5] under noise-free conditions. It must be stressed, however, that proximate sources that are simultaneously active may remain unresolved due to the low spatial resolution of MNE and weighted-MNE methods.

A cure for low spatial resolution was proposed via the use of re-weighted (iterative) minimum-norm algorithms. Specifically, the Focal Underdetermined System Solver (FOCUSS) [11,12] uses a low-resolution initial estimate that is refined through an iterative weighted-norm minimization process, aiming to find a sparse solution. The re-weighted minimum norm algorithms can be seen as a class of estimators related to Interior Point methods [13] which combine some strengths (or circumvent some pitfalls) of dipole fitting and current density approaches. For example, they do not require *a priori* information about the number of sources and retrieve sparse (focal) solutions instead of the low resolution (blurred) solutions obtained by non-iterative MNE-based strategies.

The performance of this class of iterative estimation algorithms (including the extension of FOCUSS to multiple measurement vectors, *i.e.* M-FOCUSS [14]) depends on the choice of initialization and regularization. Since a localized energy constraint does not necessarily define a unique solution, initialization may to a large degree influence the final compact solution to which the algorithm converges [12]. As such, these algorithms are vulnerable to localization bias of the MNE or nMNE when they are employed as initial estimates (as proposed in [11]) thus requiring additional compensation terms that must be estimated specifically for the sensor and head configuration geometry of each experimental

This work supported by internal funding from the University of Kansas.

M. Popescu is with the Hoglund Brain Imaging Center and the Molecular and Integrative Physiology Dept., University of Kansas Medical Center (phone: 913-588-3519; fax: 913-588-9071; e-mail: mpopescu@kumc.edu).

S.D. Blunt is with the Elec. Engr. & Comp. Sci. Dept., Univ. of Kansas (email: sdblunt@ittc.ku.edu).

T. Chan was with the Elec. Engr. & Comp. Sci. Dept., Univ. of Kansas and is now with the Elec. & Comp. Engr. Dept., Johns Hopkins University.

setup [11,15]. In addition, the choice of regularization is not trivial. Ideally, the Tikhonov regularization [16,17] or truncated SVD (TSVD, [18]) require solving an optimization problem for the regularization parameter or for the number of truncated singular values, respectively, at each iteration, which is computationally expensive. While these iterative schemes are very appealing, non-trivial implementation issues have thus far limited their use in actual MEG applications.

In this study we evaluate a new iterative algorithm that aims to improve performance in reconstructing sparse solutions for the magnetic source imaging problem. The new approach is denoted as **S**ource **AFF**ine **I**mage **RE**construction (SAFFIRE) [19]. Derived as a recursive implementation of a Minimum Mean-Square Error (MMSE) solution [20], SAFFIRE uses the affine scaling transform in an iterative scheme that is similar in nature with the one previously proposed for FOCUSS. We use theoretical and empirical results to assess the effect of initialization, and show that a simple matched filter bank can better serve this purpose compared with the regularized MNE or nMNE initializations tested in previous studies. SAFFIRE is also shown to be less sensitive to the choice of regularization in the presence of noise as it naturally contains a regularization term by virtue of being derived from the MMSE framework. Furthermore, robustness to uncertainties in the forward problem formulation (inherently present in experimental applications) is shown to be achieved by a separate adaptive regularization term arising from the MMSE structure that is adjusted according to the update of the source estimate.

II. Source Affine Image Reconstruction

A. Minimum Mean Square Error Estimation

As with many other functional brain imaging methods, SAFFIRE is predicated on the assumption that measurements of brain activity via an array of sensors around the head can be modeled as the superposition of independent contributions from M sources. Sources are modeled as current dipoles on an equidistant grid throughout the brain with each source characterized by three spatial components. For one time sample, measurements at the N sensors can be expressed as

$$\mathbf{y} = \mathbf{L}\,\mathbf{x} + \mathbf{v} \tag{1}$$

where $\mathbf{L}$ is the $N \times 3M$ transformation matrix, $\mathbf{x}$ is a $3M \times 1$ vector of dipole component strengths, and $\mathbf{v}$ is a $N \times 1$ vector of additive noise, considered henceforth to be zero-mean. The matrix $\mathbf{L}$ contains the *leadfield vectors* of the ϕ, θ, and ρ components of the M dipoles (based on a spherical coordinate system). For a spherically symmetric volume conductor, currents along the radial direction do not produce any magnetic field outside the volume conductor [21]. In this case (tested throughout this study), $\mathbf{L}$ is expressed as a $N \times 2M$ matrix that transforms the $2M \times 1$ vector $\mathbf{x}$ (comprised of strengths along the ϕ and θ components).

Based on (1), the MMSE estimation problem is solved by minimizing the standard MMSE cost function [20]

$$J = E\{\|\mathbf{x} - \hat{\mathbf{x}}\|^2\} = E\{\|\mathbf{x} - \mathbf{W}^T\mathbf{y}\|^2\} \tag{2}$$

where $E\{\bullet\}$ denotes expectation, $(\bullet)^T$ is transposition, $\hat{\mathbf{x}}$ is the MMSE estimate of $\mathbf{x}$, and $\mathbf{W}$ is the $N \times 2M$ MMSE filter bank. The cost function in (2) can be minimized by differentiating J with respect to the matrix $\mathbf{W}$ and setting the result equal to zero, yielding

$$\mathbf{W} = (E\{\mathbf{y}\,\mathbf{y}^T\})^{-1} E\{\mathbf{y}\,\mathbf{x}^T\}\,. \tag{3}$$

Substituting (1) into (3) and assuming no correlation between source signals and noise, the MMSE filter bank is

$$\mathbf{W} = (\mathbf{L}\;E\{\mathbf{x}\,\mathbf{x}^T\}\;\mathbf{L}^T + E\{\mathbf{v}\,\mathbf{v}^T\})^{-1}\;\mathbf{L}\;E\{\mathbf{x}\,\mathbf{x}^T\}\,. \tag{4}$$

The noise correlation matrix $\mathbf{R}_\mathbf{v} = E\{\mathbf{v}\,\mathbf{v}^T\}$ can be estimated for most MEG applications from the data segments in which no evoked response signal is present. Conversely, the source correlation matrix $\mathbf{P} = E\{\mathbf{x}\,\mathbf{x}^T\}$ cannot be determined *a priori*. Leveraging the direction-of-arrival (DOA) estimation method of [22,23] an iterative strategy is employed such that the MMSE filter bank of (4) is approximated as

$$\hat{\mathbf{W}}(k) = \left(\mathbf{L}\;\hat{\mathbf{P}}(k-1)\,\mathbf{L}^T + \mathbf{R}_\mathbf{v}\right)^{-1}\mathbf{L}\;\hat{\mathbf{P}}(k-1) \tag{5}$$

where

$$\hat{\mathbf{P}}(k-1) = [\hat{\mathbf{x}}(k-1)\;\;\hat{\mathbf{x}}^T(k-1)]\;\odot\;\mathbf{I} \tag{6}$$

in which $\odot$ is the Hadamard product (element-by-element multiplication) and $\mathbf{I}$ is the identity matrix. Given the MMSE filter bank estimate $\hat{\mathbf{W}}(k)$ from (5), the dipole component strength estimates at the k-th recursion is

$$\hat{\mathbf{x}}(k) = \mathbf{W}^T(k)\;\mathbf{y}\,. \tag{7}$$

Equations (5), (6), and (7) serve as the core of the SAFFIRE algorithm, upon which its specific attributes described in the following subsections are built. The recursive procedure is repeated until a stable source distribution is obtained or, to save on computation time, a hard stopping criteria (upper limit) on the number of iterations is reached [12].

B. Affine Transform of Solution Space

The norms of the columns of $\mathbf{L}$ are relatively large for regions close to the sensors causing MNE initializations to produce estimates that are biased towards superficial sources [4,5]. To partly ameliorate this problem SAFFIRE operates in an affine-transformed space in which the norm variations are removed, such as used in nMNE approaches [7].

The transform matrix $\mathbf{D}$ is formulated as

$$\mathbf{D} = ([\mathbf{L}^T\mathbf{L}]\;\odot\;\mathbf{I})^{1/2}\,, \tag{8}$$

a diagonal matrix comprised of the ℓ_2 norms of the columns of $\mathbf{L}$. The affine transform of the solution space is then achieved by re-expressing the forward model of (1) as

$$\begin{aligned}\mathbf{y} &= \mathbf{L}\,\mathbf{D}^{-1}\,\mathbf{D}\,\mathbf{x} + \mathbf{v}\\ &= \mathbf{L}_\mathrm{a}\,\mathbf{x}_\mathrm{a} + \mathbf{v}\end{aligned} \tag{9}$$

where $\mathbf{L}_{\mathrm{a}} = \mathbf{L}\,\mathbf{D}^{-1}$ has unit column norms and $\mathbf{x}_{\mathrm{a}} = \mathbf{D}\,\mathbf{x}$ contains the dipole component strengths scaled by the column norms of $\mathbf{L}$.

Within the affine transformed space, the iterative procedure of (5), (6), and (7) are applied by replacing $\hat{\mathbf{x}}(k-1)$ with $\hat{\mathbf{x}}_{\mathrm{a}}(k-1)$ and replacing $\mathbf{L}$ with $\mathbf{L}_{\mathrm{a}}$. After the terminal K-th iteration, the final estimate of the dipole component strengths can then be obtained via inverse affine transform

$$\hat{\mathbf{x}} = \mathbf{D}^{-1}\ \hat{\mathbf{x}}_{\mathrm{a}}(K). \tag{10}$$

C. Matched Filter Bank Initialization

Previous iterative approaches such as FOCUSS used MNE or nMNE initializations of the dipole component strengths. However, due to severe ill-conditioning regularization is necessary. Furthermore, MNE/nMNE may yield biased initial estimates that differ greatly from the true solution.

In contrast, SAFFIRE uses a far less ambitious initialization via an affine matched filter (MF) bank as

$$\hat{\mathbf{x}}_{\mathrm{a}}(0) = \mathbf{L}_{\mathrm{a}}^{T}\ \mathbf{y}\ . \tag{11}$$

The MF has been previously employed in *dipole scan* searches over a pre-defined source space [24]. For zero-mean additive noise, the MF provides unbiased estimators for the (scaled) strength of a single dipolar source if the leadfield vectors along each component of the dipole are orthogonal. In practice, the (normalized) leadfield vectors for orthogonal directions at the same location are not necessarily orthogonal, but their correlation generally remains small. Second, due to high correlation between columns of the leadfield matrix that correspond to similar directions at nearby locations, the MF possesses a wide mainlobe and provides rather poor spatial resolution. This property will be shown to act favorably for the iterative algorithm, since it minimizes the risk of convergence into local minima at subsequent iterations.

D. Energy Normalization

The low-resolution nature of MF spreads energy over most of the solution space due to the correlation between leadfield vectors. Subsequent application of the iterative procedure of (5), (6), and (7) then provides a recursive "soft" refinement of the spatial resolution, ideally until only the true source locations remain. However, in interim iterations the distribution of estimated source energy over many dipole components produces an intrinsic scale factor in (5) that may be $\ll 1$ and can adversely impact the relationship between the source and noise power estimates and also induce finite precision effects..

To compensate for this scaling, SAFFIRE utilizes energy normalization at each iteration to ensure that the dipole component estimate, if inserted into the forward model (exclusive of noise), would yield a received signal estimate that possesses the same energy as the actual received signal. An estimate of the received signal given the current estimate of the dipole component strengths $\hat{\mathbf{x}}_{\mathrm{a}}(k)$ is computed as

$$\hat{\mathbf{y}}(k) = \mathbf{L}_{\mathrm{a}}\ \hat{\mathbf{x}}_{\mathrm{a}}(k) \tag{12}$$

with the resulting energy estimate determined as

$$\hat{\xi}(k) = \hat{\mathbf{y}}^{T}(k)\ \hat{\mathbf{y}}(k)\ . \tag{13}$$

Given the energy of the measured signal as

$$\xi_{\mathrm{meas}} = \mathbf{y}^{T}\mathbf{y}\ , \tag{14}$$

the energy-normalized dipole component strength estimate is

$$\hat{\mathbf{x}}_{\mathrm{a,norm}}(k) = \sqrt{\xi_{\mathrm{meas}} \big/ \hat{\xi}(k)}\ \ \hat{\mathbf{x}}_{\mathrm{a}}(k) \tag{15}$$

at the k-th iteration of SAFFIRE.

E. Noise Correlation Estimation

Unlike FOCUSS or other iterative methods such as SSLOFO [25] or SIMN [26], which require the determination of a proper regularization strategy to accommodate for ill-conditioning effects and the presence of additive noise in the forward model, the MMSE formulation of SAFFIRE naturally contains a term that serves this function. Since most MEG applications employ evoked field paradigms, the noise correlation matrix $\mathbf{R}_{\mathrm{v}} = E\{\mathbf{v}\,\mathbf{v}^{T}\}$ can be estimated directly from the measured data as

$$\hat{\mathbf{R}}_{v} = \frac{1}{N_{\mathrm{noise}}} \sum_{n=1}^{N_{\mathrm{noise}}} \mathbf{y}_{n}\ \mathbf{y}_{n}^{T} \tag{16}$$

over an interval of N_{noise} time samples in which no evoked response is present, such as the pre-stimulus baseline segment.

F. Non-Coherent Integration

Assuming stationarity of the active sources over a given epoch of time samples, non-coherent integration (a rather natural generalization of the SAFFIRE algorithm that subsumes the case of a single time sample) can be used to provide greater robustness to noise. Let $\mathbf{Y}$ be the received signal vectors over Q time samples denoted as

$$\mathbf{Y} = [\ \mathbf{y}_{1}\ \ \mathbf{y}_{2}\ \ \cdots\ \ \mathbf{y}_{Q}\ ] \tag{17}$$

such that $\mathbf{Y}$ is $N \times Q$. When non-coherent integration is employed, the initialization of (11) becomes

$$\hat{\mathbf{X}}_{\mathrm{a}}(0) = \mathbf{L}_{\mathrm{a}}^{T}\ \mathbf{Y} \tag{18}$$

with $\hat{\mathbf{X}}_{\mathrm{a}}(0) = [\hat{\mathbf{x}}_{\mathrm{a},1}(0)\ \ \hat{\mathbf{x}}_{\mathrm{a},2}(0)\ \ \cdots\ \ \hat{\mathbf{x}}_{\mathrm{a},Q}(0)]$ the initial source distribution estimates for the Q time samples. Likewise, the measured energy from (14) is now defined as an average over the Q time samples as

$$\xi_{\mathrm{meas}} = \mathrm{tr}\{\mathbf{Y}^{T}\mathbf{Y}\} \tag{19}$$

where $\mathrm{tr}\{\bullet\}$ is the *trace* operation.

At each iteration, the estimation of $\hat{\mathbf{P}}(k-1)$ generalizes to

$$\hat{\mathbf{P}}(k-1) = \frac{1}{Q}[\hat{\mathbf{X}}_{\mathrm{a,norm}}(k-1)\ \ \hat{\mathbf{X}}_{\mathrm{a,norm}}^{T}(k-1)]\ \odot\ \mathbf{I}\ . \tag{20}$$

Subsequently, the application of the filter in (7) becomes

$$\hat{\mathbf{X}}_{\mathrm{a}}(k) = \hat{\mathbf{W}}^{T}(k)\ \mathbf{Y}\ . \tag{21}$$

Finally, the energy normalization procedure becomes

$$\hat{\mathbf{Y}}(k) = \mathbf{L}_{\mathrm{a}}\ \hat{\mathbf{X}}_{\mathrm{a}}(k) \tag{22}$$

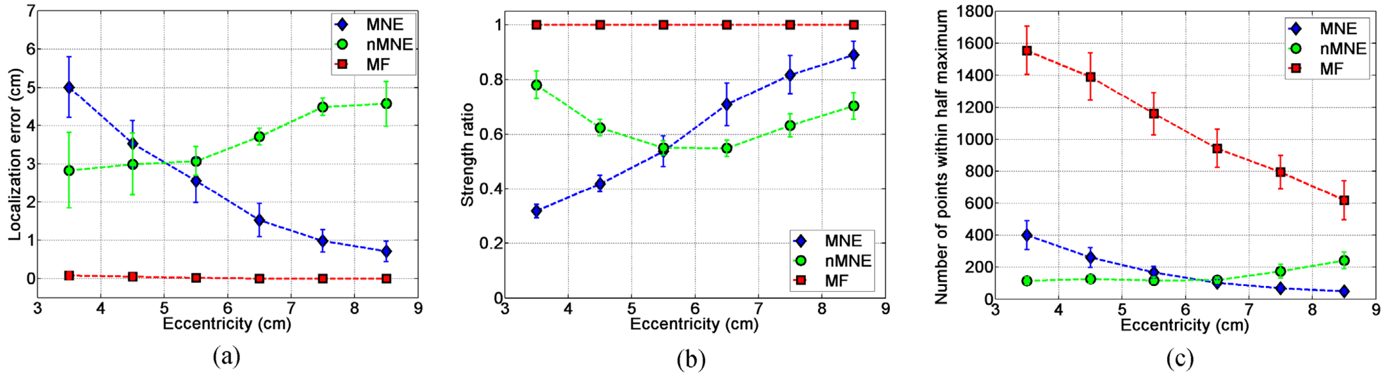

Fig. 1. Assessment of initialization for (a) localization errors, (b) strength ratio, and (c) spatial resolution.

$$\hat{\xi}(k) = \mathrm{tr}\{\hat{\mathbf{Y}}^T(k)\ \hat{\mathbf{Y}}(k)\}\,, \tag{23}$$

and

$$\hat{\mathbf{X}}_{\mathrm{a,norm}}(k) = \sqrt{\xi_{\mathrm{meas}} / \hat{\xi}(k)}\ \hat{\mathbf{X}}_{\mathrm{a}}(k)\,. \tag{24}$$

The terminal inverse affine transform is performed as

$$\hat{\mathbf{X}} = \mathbf{D}^{-1}\ \hat{\mathbf{X}}_{\mathrm{a}}(K) \tag{25}$$

The normalization $1/Q$ in (20) ensures that the signal and noise terms in the MMSE filter retain the same relationship as in the measured data. Except for this normalization, the non-coherent integration procedure is equivalent to the Frobenius norm approach of M-FOCUSS [14]. Optionally, an estimate of signal power over the stationary interval can be obtained as

$$\left\langle \hat{\mathbf{x}}^2 \right\rangle = \sum_{q=1}^{Q} \hat{\mathbf{x}}_q \odot \hat{\mathbf{x}}_q\ . \tag{26}$$

G. *Treatment of Forward Model Uncertainties*

While simulation studies typically assume perfect knowledge of the leadfield matrix in (1), such an assumption is not valid for real MEG applications. Forward problem uncertainties can arise due to approximation of the volume conductor, the limited accuracy of co-registration, and discretization of the source space. These factors necessitate a separate treatment of modeling errors for an iterative method to provide sensible solutions in real MEG experiments.

To account for modeling errors, we generalize (1) as

$$\mathbf{y} = (\mathbf{L}_{\mathrm{a}}\mathbf{x}_{\mathrm{a}}) \odot \mathbf{z} + \mathbf{v} \tag{27}$$

where the $N \times 1$ vector $\mathbf{z}$ incorporates (unknown isotropic) modeling errors. The n-th element of $\mathbf{z}$ is generally modeled as

$$z_n = 1 + \Delta l_n \tag{28}$$

where Δl_n is a random amplitude deviation of arbitrary distribution that characterizes the effect of the modeling errors in the n-th sensor. Thus, (27) can be written as

$$\mathbf{y} = \mathbf{L}_{\mathrm{a}}\mathbf{x}_{\mathrm{a}} + \mathbf{v} + \mathbf{v}_z\,, \tag{29}$$

where $\mathbf{v}_z = (\mathbf{L}_{\mathrm{a}}\mathbf{x}_{\mathrm{a}}) \odot (\mathbf{z} - \mathbf{1}_{N\times 1})$ is a "model noise" vector induced by the presence of the modeling errors. Based on the assumption that the modeling errors are i.i.d. across the sensors and their distribution is zero-mean and symmetric we can define the variance of z_n as σ_z^2 (the same for all sensors). Substituting (29) into (3) and assuming that the source signals and additive noise are statistically independent, it can easily be shown that the MMSE filter from (4) becomes

$$\mathbf{W} = (\mathbf{L}_{\mathrm{a}}\, E\{\mathbf{x}_{\mathrm{a}}\mathbf{x}_{\mathrm{a}}^T\}\mathbf{L}_{\mathrm{a}}^T + E\{\mathbf{v}\mathbf{v}^T\} + E\{\mathbf{v}_z\mathbf{v}_z^T\})^{-1}\ \mathbf{L}_{\mathrm{a}}\, E\{\mathbf{x}_{\mathrm{a}}\mathbf{x}_{\mathrm{a}}^T\}\,. \tag{30}$$

The "model noise" covariance $\mathbf{R}_z = E\{\mathbf{v}_z\mathbf{v}_z^T\}$ in (30) is an additional loading term that accounts for uncertainties in the forward model. Substituting in the model noise yields

$$\begin{aligned}\mathbf{R}_z &= E\{(\mathbf{z} - \mathbf{1}_{N\times 1}) \odot (\mathbf{L}_{\mathrm{a}}\mathbf{x}_{\mathrm{a}})(\mathbf{L}_{\mathrm{a}}\mathbf{x}_{\mathrm{a}})^T \odot (\mathbf{z} - \mathbf{1}_{N\times 1})^T\} \\ &= E\{\tilde{\mathbf{Z}}\,(\mathbf{L}_{\mathrm{a}}\mathbf{x}_{\mathrm{a}})(\mathbf{L}_{\mathrm{a}}\mathbf{x}_{\mathrm{a}})^T\tilde{\mathbf{Z}}^T\}\end{aligned}\,, \tag{31}$$

where $\tilde{\mathbf{Z}} = diag\{z_0, z_1, \ldots, z_n\} - \mathbf{I}_{N\times N}$. Using the assumptions of source signal and modeling error independence and uncorrelated modeling errors, (31) simplifies to

$$\mathbf{R}_z(k) = \sigma_z^2\, \mathbf{I}_{N\times N} \odot (\mathbf{L}_{\mathrm{a}}\ \mathbf{P}(k)\, \mathbf{L}_{\mathrm{a}}^T)\,. \tag{32}$$

The filter bank update is thus

$$\hat{\mathbf{W}}(k) = (\mathbf{L}_{\mathrm{a}}\ \hat{\mathbf{P}}(k-1)\mathbf{L}_{\mathrm{a}}^T + \hat{\mathbf{R}}_z(k-1) + \mathbf{R}_{\mathbf{v}})^{-1}\ \mathbf{L}_{\mathrm{a}}\ \hat{\mathbf{P}}(k-1)\,. \tag{33}$$

Equation (33) indicates that, while $\mathbf{R}_{\mathbf{v}}$ represents a fixed regularization term, the model noise covariance $\mathbf{R}_z(k)$ is a signal-dependent term that adapts according to the update of the source estimates. The impact of modeling errors can be adjusted via the σ_z parameter which, according to (27) and (28), can be regarded as an expected *relative* error in the sensor measurements due to the use of imperfect physical models. Based on this, and on empirical observations, values of σ_z in the range of 5% to 10% (*i.e.* 0.05 to 0.1 relative to 1 in (28)) lead to good performance of the algorithm when applied to real data (exemplified in Section IV).

III. Simulation Results

Using simulation experiments, we first compare MF initialization with MNE and nMNE solutions to determine the location, weighting bias, and initial resolution. We then assess the quality of the final SAFFIRE solution as a function of the manner of initialization. Finally, SAFFIRE is compared with the MNE, nMNE, and FOCUSS for the reconstruction of distant and proximal pairs of correlated sources.

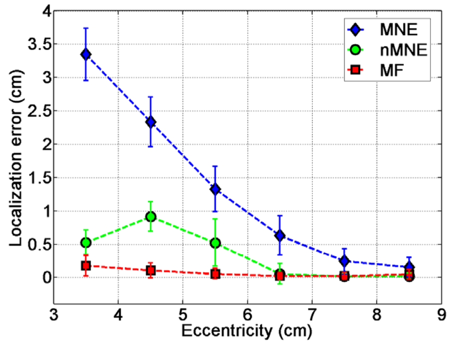

(a)

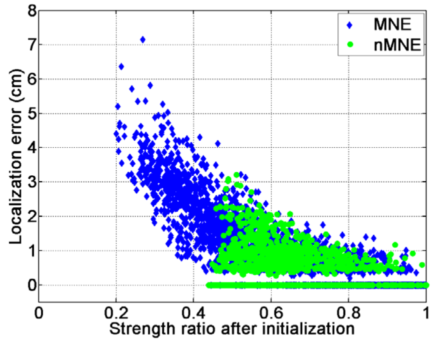

(b)

Fig. 2. (a) SAFFIRE localization error for different initializations. (b) Dependence of SAFFIRE final localization error on the strength ratio after initialization with MNE and nMNE.

A. *Effects of Different Initialization Schemes*

The first set of simulation experiments address properties of the different initializations. One dipolar source was independently considered at various positions within a regular, three-dimensional grid of support points (9014 locations spaced at an averaged distance of 5 mm). This grid provides a uniform coverage of the brain compartment segmented from T1-weighted MRI data from a participant in one of our MEG studies. The dipole orientations were set along each of the two tangential directions of a spherical volume conductor model fitted to the subject's head. The temporal dipole activation was simulated as a Gaussian curve with 150 ms width and peak strength of 30 nAm. The simulated magnetic field was computed at the sensor positions of the 151 channel CTF Omega system (VSM MedTech, Vancouver, Canada) using the Sarvas equations for non-radial magnetic measurements [27]. The leadfield matrix was computed for axial gradiometer sensors with 5 cm distance between lower and upper coils. White noise with RMS value of 10 fT was added to the simulated data, and a noise-only temporal window of 0.5 sec was appended to allow for the estimation of the noise correlation. The SNR at the peak dipole strength varied between approximately 3 (~5 dB) and 225 (~24 dB) when the dipole position was varied across all nodes of the source grid.

The inverse solution was evaluated at the peak-latency using three initialization approaches: regularized MNE, regularized nMNE, and affine-transformed MF bank. The regularized MNE solution has been obtained via [8] as

$$\mathbf{x}_{MNE} = \tilde{\mathbf{L}}^T (\tilde{\mathbf{L}}\tilde{\mathbf{L}}^T + \lambda^2 \mathbf{I})^{-1} \tilde{\mathbf{y}} \qquad (34)$$

where $\tilde{\mathbf{y}} = \mathbf{R}_\mathbf{v}^{-1/2}\mathbf{y}$ and $\tilde{\mathbf{L}} = \mathbf{R}_\mathbf{v}^{-1/2}\mathbf{L}$ are the spatially whitened data and leadfield matrices, respectively. The regularization parameter was set to $\lambda^2 = \delta^2\, tr(\tilde{\mathbf{L}}\tilde{\mathbf{L}}^T)/N$ with δ^2 the inverse of the power SNR of the whitened data. The nMNE was used with a component-wise normalization at every location.

We evaluated the initializations using three metrics: localization error, which is defined as the Euclidian distance between the location of the simulated dipole and the spatial peak-strength of the solution; the ratio of the absolute strength at the position of the simulated dipole to the spatial peak of the solution (characterizing the weight bias at initialization); and the number of dipoles with reconstructed amplitudes exceeding more than 50% of the maximum amplitude as a measure of the spatial smoothness (half-maximum volume).

As expected, the MNE retrieved increasingly biased solutions (Fig. 1a) accompanied by a decrease in spatial resolution (Fig. 1c) as source eccentricities become smaller. Incorrect localizations of deep sources are accompanied by heavily unbalanced weighting (Fig. 1b), which acts to increase the risk of convergence into local minima at subsequent iterations. Due to overcompensation, the improvement observed for nMNE is essentially limited to the localization of deep sources. In contrast, the MF provides consistent results (Figs. 1a and 1b), manifesting only a slight degradation for some sources positioned at small eccentricities (due to the small SNR). The relatively good localization accuracy, however, is accompanied by the extremely low spatial resolution (Fig. 1c), which explains why such an approach is not generally employed in isolation for MEG/EEG imaging.

B. *Propagation of Initialization Effects*

SAFFIRE was evaluated with each of the three initializations to assess how initialization effects propagate through the iterations. The convergence criterion was based on the rotationally invariant Euclidian length of the current at each position [15]. To avoid the summed contribution of a large number of negligible magnitude currents, we considered a cost function based only on the union of locations with source power higher than 0.5% of the maxima at the previous and current iterations. The convergence criterion was achieved when the relative total power change at these locations was lower than 0.05%. The algorithm was stopped when the convergence criterion was met or when a maximum number of 25 iterations was reached.

Fig. 2a illustrates the localization errors of SAFFIRE with different initializations. As a global characterization, perfect (zero error) localization was achieved in 23.6% (MNE), 64.8% (nMNE), and 89.2% (MF) of conditions. Also, a minimal localization error of one source space point was achieved in 21.1% (MNE), 15.0% (nMNE), and 9.4% (MF) of conditions. Using MF initialization, the average number of iterations needed to achieve convergence was 15.7 (SD=3.8), with an observed trend of slightly fewer iterations for sources at larger eccentricities. In terms of smoothness of the final solution, the half-maximum volume was confined to a single source space point in 93.2% of conditions, with the rest of conditions being characterized by two (6.3%) and three (0.5%) grid points. The maximum number of iterations 25 was

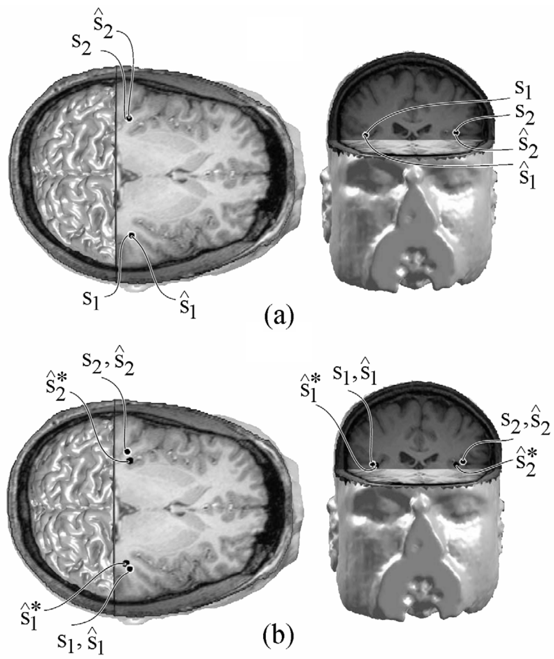

Fig. 3. SAFFIRE with one time sample for distant correlated sources. Results are shown for 50% (a) and 20% (b) clipping thresholds.

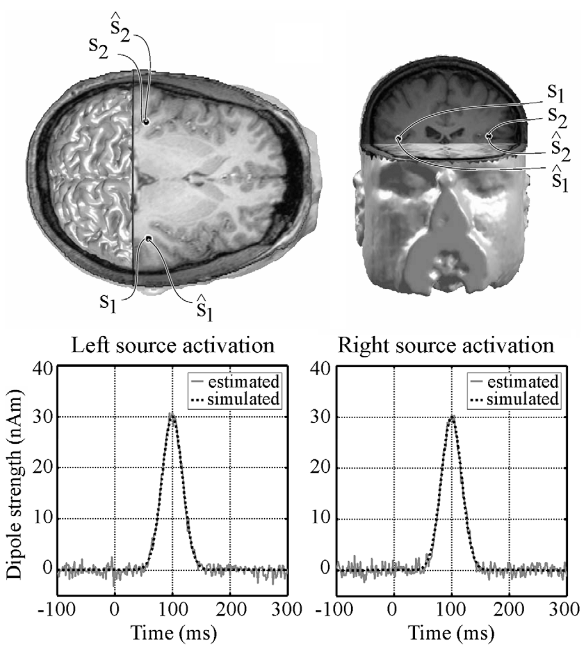

Fig. 4. SAFFIRE with non-coherent integration of 4 time samples for distant correlated sources. Upper panel results are shown for 1% threshold.

reached in 14.6% of conditions (with a high incidence of conditions with low SNR). Among these, perfect localization was still achieved in 81.6% of the time. A closer inspection of cases when the upper limit of iterations was reached indicated that positions of significant estimated strength are always stable during the last iterations, and the convergence criterion was not met only because of small amplitude variations.

For MNE initialization, SAFFIRE performance qualitatively replicates MNE behavior, with increasingly higher errors for smaller eccentricities, though the mean localization errors are smaller than those immediately after initialization. Compared to MNE, the nMNE initialization proves to be a better choice over all eccentricities. This is surprising for high eccentricities, where nMNE provides initializations with increased mean localization errors (Fig. 1a) and moderately lower mean strength ratios (Fig. 1b). This result can be explained by the lower resolution of nMNE compared to MNE at large eccentricities (Fig. 1c) which is beneficial for the iterative algorithm by enabling more freedom to correct for the initial error. Note that a similar result does not occur for the lower resolution of MNE at small eccentricities. The localization bias, which is associated with smaller strength ratios after MNE initialization, cannot be corrected during subsequent iterations. The strength ratios for nMNE are generally confined to a range of moderate values, remaining higher than 40% when the simulated source was varied across the source space. By comparison, the strength ratios for MNE take on much lower values thus imposing a heavier penalty on the real sources after initialization. Progressively lower strength ratios are associated with a steepest increase in localization errors after convergence (Fig. 2b).

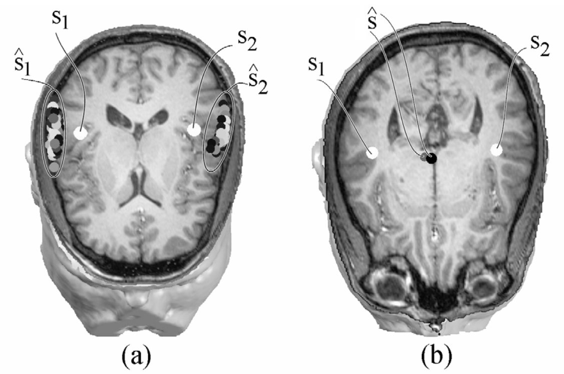

Fig. 5. Reconstruction using regularized MNE (a) and nMNE (b) for two distant sources. Results are shown for 50% clipping thresholds.

Several conclusions of practical importance can be drawn from these results. First, bias introduced by MNE and nMNE can sometimes be corrected during subsequent iterations. This observation confirms that the iterative algorithm does not simply reinforce the sources with the largest strength after initialization, which was also pointed out in [11,12]. Second, initialization errors can, however, propagate in some cases, thus leading to erroneous convergence to local minima. Third, a lower resolution initial estimate favors convergence to the correct solution despite possible bias at initialization, provided that the relative strength penalty imposed by the initial estimate on the true source is not excessively large.

Based on these observations, the motivation for MF initialization is twofold: it provides low resolution estimates and it reduces the risk of a large strength penalty on the true source. Due to these properties, MF can alleviate the vulnerability of iterative algorithms to the effects of MNE or nMNE initializations. Since the MF is particularly suited for modeling the single dipole scenario, its superior performance in these preliminary tests is expected; how this performance extends to more complex scenarios is addressed in the next sections.

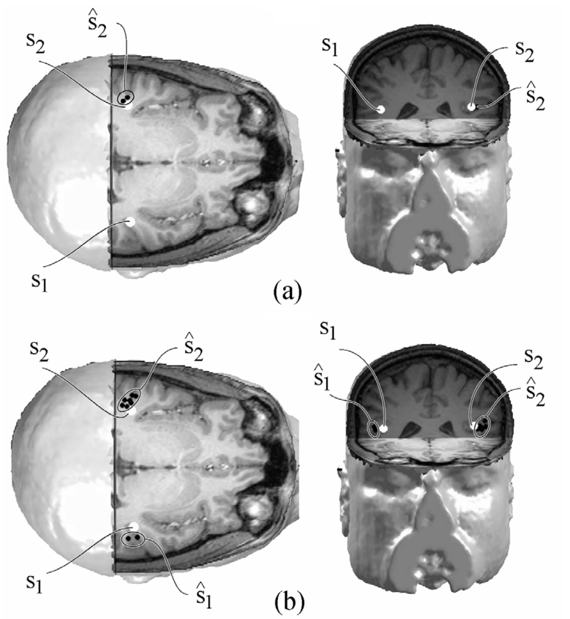

Fig. 6. FOCUSS results for two distant sources are shown at 50% (a) and 20% (b) clipping thresholds.

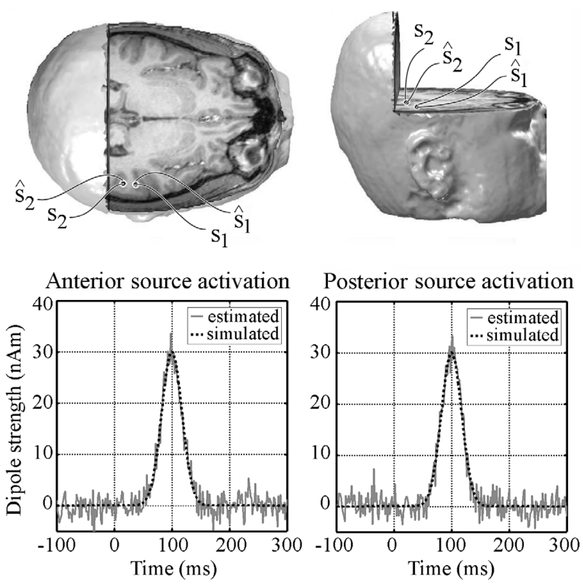

Fig. 7. SAFFIRE with non-coherent integration of 4 time samples for proximal sources. Upper panel results are shown for 1% threshold.

C. *Evaluation for Dipole Pairs*

We now exemplify SAFFIRE performance for the reconstruction of a distant/proximal pair of correlated sources. The first simulation experiment assumes two dipoles positioned within deep regions of the auditory cortex in each of the brain hemispheres with a source separation of 8.3 cm. Each dipole is oriented along the local declination direction and the temporal activations (derived from a Gaussian function peaking at 100 ms with a peak strength of 30 nAm) are fully correlated. Zero-mean random noise is added to the simulated MEG data with RMS noise level of 10 fT.

Fig. 3 illustrates the source localization using SAFFIRE with 1 time sample at the peak of the dipoles activity and for two clipping thresholds: 50% and 20% of the maximum

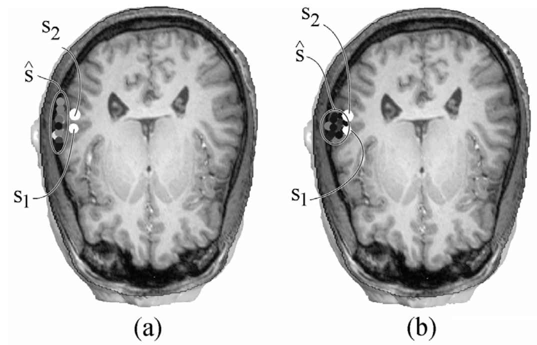

Fig. 8. Reconstruction using regularized MNE (a) and nMNE (b) for two proximal sources. Results are shown for 50% clipping thresholds.

reconstructed strength, respectively. Simulated (s) and reconstructed ($\hat{s}$) sources are annotated to aid visualization (s^* denotes additional reconstructed sources, visible only at the low clipping threshold). The simulated source positions are shown as white dots. The results demonstrate that the energy of the reconstructed sources is very focal and in the correct positions. Only a small fraction of the sources' power is retrieved at a nearby point for each of the simulated sources.

Fig. 4. demonstrates the higher resolution and greater robustness to noise that SAFFIRE can achieve using the non-coherent integration procedure (4 time samples). The reconstructed time-courses of activity for each of the two sources also indicate very good estimation accuracy.

For comparison, Fig. 5 illustrates the results of regularized MNE (a) and nMNE (b) algorithms. Tikhonov regularization was used with the optimum regularization parameter estimated by the L-curve method [28]. The results indicate the characteristic bias of MNE towards superficial sources (shifted in the medio-lateral direction, closer to the sensors), as well as its over-smoothing effect. The nMNE results indicate that leadfield normalization is vulnerable to an over-compensation bias for deep sources near the center of the volume conductor.

The FOCUSS results are shown in Fig. 6 where the weight matrix in each iteration has been obtained from the compound product of all preceding solutions [11]. MNE initialization was used and a truncated SVD scheme was applied using the 30 highest singular values. This version of FOCUSS provides a sparse solution, thus improving the localization accuracy with respect to MNE. However, it cannot achieve the same localization accuracy as SAFFIRE. It should be noted that when the nMNE initialization was used instead of MNE, the solution was shifted to very deep brain regions, indicating that at subsequent iterations the initialization bias (Fig. 5b) is not corrected. The FOCUSS results are qualitatively similar to those obtained when MNE and nMNE, respectively, were used to initialize SAFFIRE. Thus, despite all other differences between the two algorithms, this observation indicates that *initialization* has a major impact on final solution accuracy.

The second experiment exemplifies the ability of the different algorithms to localize two proximal sources. Two dipoles with positions within regions of the auditory cortex and essentially parallel orientations were simulated with a separation of 1.1 cm where the temporal courses of the dipoles activations are the same as before. The version of SAFFIRE

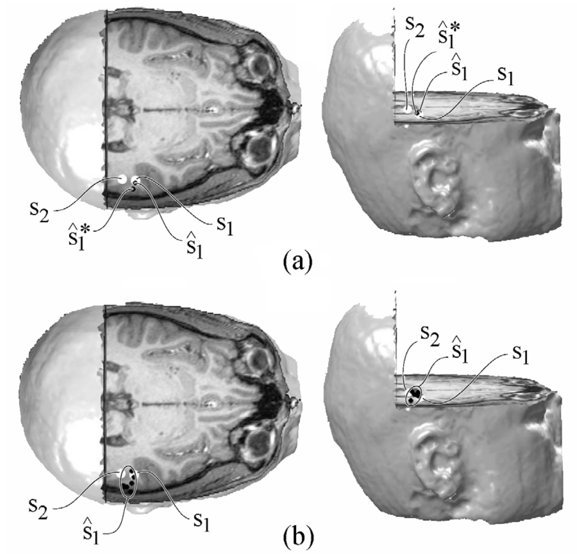

Fig. 9. FOCUSS results for two proximal sources are shown at 50% (a) and 20% (b) clipping thresholds.

that employs non-coherent integration across 4 time samples retrieves a perfect estimate of the two sources, without any significant energy spread across adjacent locations (Fig. 7). In contrast, regularized MNE (with or without normalization) does not reliably indicate the existence of two separate sources (Fig. 8). This observation holds also for the version of the FOCUSS algorithm tested here (Fig. 9), which was able to localize only one dipolar source with acceptable accuracy.

IV. Application to Real MEG Data

A. Data Acquisition and Processing

The performance of SAFFIRE is exemplified on MEG data from a tactile somatosensory experiment. The experimental paradigm employs cutaneous stimuli delivered by modulating the pressure of a silicone Soothie™ pacifier receiver yielding a 275 µm deflection with each stimulus. In one session the stimulus probe was positioned at the glabrous surface of the right hand, between the thumb, index, and middle finger (condition 1, hand stimulation), while in the second session the probe was placed at the midline between the vermilion surface of the upper and lower lips (condition 2, lips stimulation). For each stimulation site, the tactile stimuli (50 ms duration) were delivered in 125 trials, with an inter-trial interval of 5s.

Co-registration with the T1-weighted MRI, acquired after the MEG experiment, was done using localization coils/ registration landmarks placed at nasion, left, and right pre-auricular points. The source space was a regular grid of points (4 mm average separation) throughout the brain. Leadfield matrices were computed for a spherical volume conductor fitted to the subject's head.

The MEG signals were acquired with a sampling rate of 600 Hz and bandpass filtered between 1.5 and 50 Hz. Artifact-free epochs were averaged separately for each session and the DC was offset using the pre-stimulus period as a baseline. Additionally, the responses from the two stimulation conditions were summed to create a third ("test") dataset to replicate a more complex scenario in which sources evoked by the hand and lips stimulation would be simultaneously active. The ability of a reconstruction algorithm to estimate the brain sources on this "test" dataset is evaluated as a prerequisite for application on real data from simultaneous tactile stimulation at multiple sites, where mislocalization of the independent sources could be misinterpreted as physiological interactions.

B. Results for Real MEG Data

Figure 10 (left panels) illustrates the averaged SEF data for the hand (a) and lips (b) stimulation, as well as the combined response created for the "test" dataset (c), as explained above. The dominant response components occur at a latency of 59 ms (hand) and 48 ms (lips), respectively. The shorter response latency for the orofacial stimulation is consistent with a shorter conduction delay for the trigeminal pathway. To allow for a direct comparison between source reconstruction in the hand and lips stimulation conditions with that from the "test" dataset, we consider the latency of 53 ms, *i.e.* between the peak responses in the two separate conditions. For hand stimulation, the magnetic field topography exhibits a dipolar pattern in sensors over the left hemisphere, *i.e.* contralateral to the stimulation site (Fig. 10a, middle panel). For lips stimulation, the magnetic field exhibits two dipolar patterns, each expanding across a sub-array of sensors covering one hemisphere and indicating the presence of bilateral neural generators (Fig. 10b, middle panel).

SAFFIRE was applied with 5 time samples via non-coherent integration (*i.e.* 2 samples before and after the selected latency), and a model error parameter $\sigma_z = 0.075$. The noise correlation was estimated from pre-stimulus segments over -1.5 s to -0.2 s. Estimated RMS noise was 12.0 fT (hand), 12.6 fT (lips), and 18.0 fT (combined).

For hand stimulation, SAFFIRE retrieves a dominant source in the hand primary somatosensory cortex (S1), on the contralateral (left) postcentral gyrus (upper part of its anterior wall), which most likely indicates activity in proximal neuronal populations from hand areas 3b and 1 (Fig. 10a, right panel). For lips stimulation, SAFFIRE retrieves bilateral activations within regions of the postcentral gyrus of the left and right hemispheres (Fig. 10b, right panel). Relative to the hand S1, the estimated left source evoked by lips stimulation was shifted laterally (3.6 mm), anteriorly (3.2 mm), and inferiorly (24 mm). These results agree with the somatotopic organization of the primary somatosensory cortex [29], with lips structures represented near the base of the postcentral gyrus with respect to the hand S1. For each of the stimulation conditions, MNE provides smoother solutions with spatial peaks located in regions proximal to the sources retrieved by SAFFIRE. MNE also retrieves spurious activity at the superficial midline.

For the "test" dataset, SAFFIRE reconstructed each of the three sources with good accuracy, reflected in the maximum difference relative to the independent localizations of only one grid point (Fig. 10c). This performance was achieved despite three adverse factors: simultaneous activity of more sources, higher noise level in the compound data, and the fact that the leadfield matrix was computed for the sensor setup of one

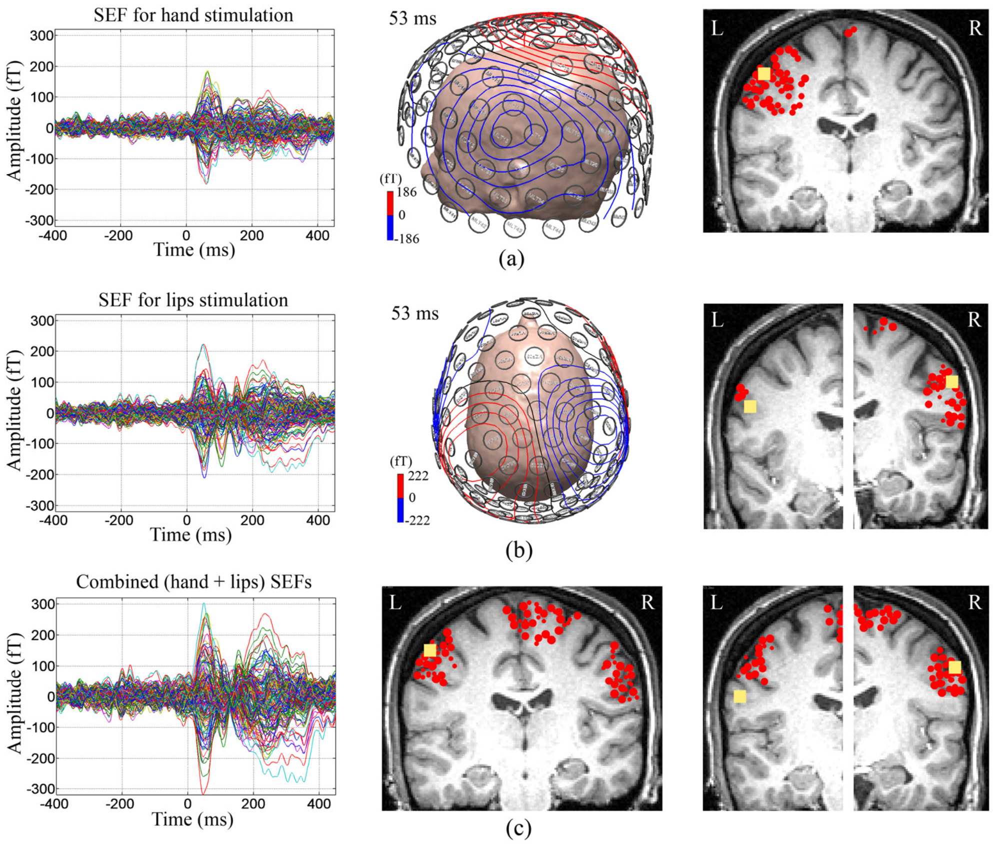

Fig. 10. SAFFIRE performance on MEG data from tactile stimulation of (a) hand, (b) lips, and (c) compound "test" data after summation of the independent responses. SAFFIRE results are shown with yellow square symbols. MNE results are shown with red dots.

stimulation condition, thus incorporating additional error due to different head positioning between the recordings (mean distance of 4.5 mm between corresponding localization coils in the two recordings). By comparison, MNE pinpoints the right hemisphere source but cannot separate the two sources in the post-central gyrus of the left hemisphere, retrieving only one spatial peak in that region.

Note that the version of FOCUSS tested in this study failed to provide a meaningful solution for this more complex source configuration scenario, and so did the simplified version of SAFFIRE (*i.e.* as given in (5)) which does not address the presence of modeling errors. In practice, for current density methods like MNE, nMNE or sLORETA the modeling errors may not constitute a significant separate issue due to the inherent smoothness of the solution. However, this result demonstrates that iterative algorithms aiming to provide focal solutions are sensitive to forward problem approximations, and underlines the necessity to address the specific role of this factor in studies intended to assess their performance.

V. Discussion

This study proposes a new iterative scheme for MEG source reconstruction, seeking to address the sensitivity of previously proposed methods to initialization and regularization strategy, as well as to uncertainties in forward problem formulation that can affect performance in real applications. SAFFIRE is derived as a recursive implementation of a MMSE estimator and uses a MF initialization. The MF provides low initial resolution which favors convergence into the correct sparse solution. While MNE, nMNE, and sLORETA (employed by SSLOFO [25]) require regularized solutions to solve the ill-conditioned inverse problem, the MF approach eliminates this need and requires only an energy normalization procedure which must be an integral part of the iterative algorithm.

SAFFIRE operates in an affine-transformed space where norm variations are removed. While for non-iterative methods (*e.g.* nMNE) such an equalization approach does not suffice to correct for localization bias throughout the source space [5,7,8], our results indicate that leadfield normalization appears to be an effective general solution for SAFFIRE.

Being derived from a MMSE estimator, SAFFIRE naturally contains a noise term that serves as regularization of the solution, thus eliminating the need to solve a dual optimization problem at each iteration. The majority of MEG applications rely on evoked potential paradigms and allow for estimation of the noise correlation from a noise-only temporal window in the pre-stimulus segment. It should be stressed, however, that a regularization scheme evaluated with simulation studies which are free of leadfield estimation errors, does not necessarily remain optimal in real applications, which are inherently susceptible to forward problem uncertainties arising from approximations of the volume conductor and imperfect co-registration. To address this important issue, we showed that a separate, signal-dependent regularization term (which adapts based on the update of the source estimate) can be derived within the MMSE framework. The impact of this regularization term is readily adjusted via a model-error parameter, whose values in a relatively narrow range were observed to ensure good performance for real applications.

Non-coherent integration can be used as part of SAFFIRE to increase the resolution of the final solution as well as robustness to additive noise. Non-coherent integration assumes stationarity of active brain sources over an interval of time. Such an assumption may not be realistic over long temporal windows. However, even 3-5 time samples (given a reasonable sampling rate of the data) can provide superior results (supported by the examples presented in this study) that recommend it as an integral part of the algorithm.

Although far from being exhaustive, the evaluation results described in this study indicate that SAFFIRE could be a promising method for source estimation in MEG. Other studies [25,26] have also proposed alternative ways to improve the performance of this class of iterative algorithms. In particular, SSLOFO [25] proposed the use of sLORETA [10] as the initialization step. Since sLORETA also provides a spatially smooth initial solution, the overall effects of such an initialization could be similar in many scenarios to those observed in our study for MF initialization, although a definitive answer await conclusions of future studies. SSLOFO, like FOCUSS, is more sensitive than SAFFIRE to the choice of several parameters, and the effect of some of them on overall performance has yet to be fully characterized. Particularly, SSLOFO involves shrinking of the number of grid points at each iteration, requiring a definition of the shape and size of the regions of interest, which may need to be application specific [25]. The sensitivity to this choice and the regularization strategy may explain why for single sources in the presence of noise there is a slight deterioration in accuracy after convergence with respect to initial localization accuracy [25,26], or performance discrepancies reported in the original study [25] and a subsequent study that used it as a benchmark [26]. Thus, comparative evaluations between SAFFIRE and SSLOFO with source configurations replicating realistic scenarios, as well as evaluation of the accuracy and stability of the solutions at different SNRs and in the presence of forward problem uncertainties await future studies.

Acknowledgment

The authors thank Dr. Steven Barlow (Dept. of Speech-Language-Hearing: Sciences & Disorders at the University of Kansas) for permission to use the somatosensory MEG data.

References

[1] H. Helmholtz, "Ueber einige Gesetze der Vertheilung elektrischer Strome in korperlichen Leitern, mit Anwendung auf die thierischelektrischen Versuche," *Ann. Phys. Chem.*, 89, pp. 211–233, pp. 353–377, 1853.

[2] M.S. Hämäläinen and R.J. Ilmoniemi, "Interpreting measured magnetic fields of the brain: estimates of current distributions". Technical Report, Helsinki University of Technology, TKK-F-A559, 1984.

[3] M.S. Hämäläinen and R.J. Ilmoniemi, "Interpreting magnetic fields of the brain: minimum norm estimates," *Med Biol Eng Comput,* v. 32, pp. 35-42, 1994.

[4] B. Jeffs, R. Leahy, and M. Singh, "An evaluation of methods for neuromagnetic image reconstruction," *IEEE Trans. Biomed. Eng.,* v. 34, pp. 713–723, 1987.

[5] K. Sekihara, M. Sahani, and S. Nagarajan, "Localization bias and spatial resolution of adaptive and non-adaptive spatial filters for MEG source reconstruction," *Neuroimage,* v. 25, pp. 1056-1067, 2005.

[6] M. Fuchs, H.A. Wischmann, and M. Wagner, "Generalized minimum norm least squares reconstruction algorithms," In Skrandies W., ed. ISBET Newsletter 5, Giessen, Germany, 8-11, 1994.

[7] M. Fuchs, M. Wagner, T. Köhler, and H.A. Wischmann, "Linear and nonlinear current density reconstructions," *J. Clin. Neurophysiol.,* v. 16, pp. 267–295, 1999.

[8] F.H. Lin, T. Witzel, S.P. Ahlfors, S.M. Stufflebeam, J.W. Belliveau, and M.S. Hämäläinen, "Assessing and improving the spatial accuracy in MEG source localization by depth-weighted minimum-norm estimates," *Neuroimage,* v. 31, pp. 160-171, 2006.

[9] A.M. Dale, A.K. Liu, B.R. Fischl, R.L. Buckner, J.W. Belliveau, J.D. Lewine, and E. Halgren, "Dynamic statistical parametric mapping: combining fMRI and MEG for high-resolution imaging of cortical activity," *Neuron,* v. 26, pp. 55– 67, 2000.

[10] R.D. Pascual-Marqui, "Standardized low resolution brain electromagnetic tomography (sLORETA): technical details," *Methods Find. Exp. Clin. Pharmacol.,* v. 24, pp. 5 –12, 2002.

[11] I.F. Gorodnitsky, J.S. George, and B.D. Rao, "Neuromagnetic source imaging with FOCUSS: a recursive weighted minimum norm algorithm," *Electroenceph. Clin. Neurophys.,* v. 95, pp. 231-251, 1995.

[12] I.F. Gorodnitsky and B.D. Rao, "Sparse Signal Reconstruction from Limited Data Using FOCUSS: A Re-weighted Minimum Norm Algorithm," *IEEE Trans. Signal Proc.*, v. 45, pp. 600–616, 1997.

[13] C. Roos, T. Terlaky, and J.-P. Vial, *Interior Point Methods for Linear Optimization*, Springer, New York, NY, 2006.

[14] S.F. Cotter, B.D. Rao, K. Engan, and K. Kreutz-Delgado, "Sparse solutions to linear inverse problems with multiple measurement vectors," *IEEE Trans. Signal Proc.*, v. 53, pp. 2477-2488, July 2005.

[15] J.G. Taylor, A.A. Ioannides, and H.W. Muller-Gartner, "Mathematical analysis of leadfield expansions," *IEEE Trans. Medical Imaging*, v. 18, pp. 151-163, Feb 1999.

[16] M. Foster, "An application of the Wiener-Kolmogorov smoothing theory to matrix inversion," *J. SIAM*, v. 9, pp. 387–392, 1961.

[17] A.N.Tikhonov, "Regularization of incorrectly posed problems," Soviet Math., 4: 1624-1627, 1963.

[18] C. Lawson, and R. Hanson, *Solving Least-Squares Problems*, Prentice-Hall, Englewood Cliffs, NJ.

[19] S.D. Blunt, T. Chan, and M. Popescu, "Source affine image reconstruction (SAFFIRE) for EEG/MEG imaging," patent pending, app. serial no. 11/837,243.

[20] S.M. Kay, *Fundamentals of Statistical Signal Processing: Estimation Theory*, Prentice Hall: Upper Saddle River, NJ, 1993, Chapter 12.

[21] R.J. Ilmoniemi, M.S. Hämäläinen, and J. Knuutila, "The forward and inverse problems in the spherical model," in *Biomagnetism: Applications and Theory*, Weinberg, Stroink, and Katila, Eds. New York: Pergamon, 1985, pp. 278–282.

[22] S.D. Blunt, T. Chan, and K. Gerlach, "A new framework for direction-of-arrival estimation," *IEEE SAM Workshop*, July 21-23, 2008.

[23] S.D. Blunt, T. Chan, and K. Gerlach, "Robust DOA estimation: the re-iterative super-resolution (RISR) algorithm," to appear *IEEE Trans. Aerospace & Electronic Systems*.

[24] M. Fuchs, M. Wagner, H.A. Wischmann, K. Ottenberg, and O. Doessel, "Possibilities of functional brain imaging using a combination of MEG and MRT," In: C. Pantev, editor, "Oscillatory event-related brain dynamics." New York: Plenum Press, pp. 435-457, 1994.

[25] H. Liu, P.H. Schimpf, G. Dong, X. Gao, F. Yang, and S. Gao, "Standardized shrinking LORETA-FOCUSS (SSLOFO): a new algorithm for spatio-temporal EEG source reconstruction," *IEEE Trans. Biomed. Eng.*, v. 52, pp. 1681–1691, Oct. 2005.

[26] W.K. Liang and M.S. Wang, "Source reconstruction of brain electromagnetic fields-source iteration of minimum norm (SIMN)," *Neuroimage,* v. 47, pp. 1301-1311, 2009.

[27] J. Sarvas, "Basic mathematical and electromagnetic concepts of the bio-magnetic inverse problems," *Phys. Med. Bio*, v. 32, pp.11-22, Jan 1987.

[28] P.C. Hansen, "Analysis of discrete ill-posed problems by means of l-curve," *SIAM Rev.*, v. 34, pp. 561–580, 1992.

[29] W. Penfield, T. Rasmussen, "The cerebral cortex of man". New York: Hafner Publishing Co, 1968.